Behavior of a Very Large Number of Constant-Volume Trajectories

FEDOR MESINGER
National Center for Atmospheric Research, Boulder, Colo., and University of Belgrade, Yugoslavia

(Manuscript received 2 March 1965)

ABSTRACT

A numerical experiment is performed with the purpose of investigating the behavior of the trajectories of a very large number of constant-volume particles. Practical significance is given to this problem by the possibility of using superpressured, constant-volume balloons for routine upper air observations.

The computational scheme of the experiment is described with emphasis on some aspects of trajectory computations. Thirty-day diagnostic trajectories are computed for two levels using the total velocity components, and for one level using only the nondivergent ones, and the resulting spacing of the trajectory points is discussed. Theory of the distances to the nearest among a large number of points is developed and applied for the statistical description of the results. Histograms of distances from the constant-volume particles as well as from random points in space to the nearest neighboring constant-volume particle are computed, and compared with the frequency function of those distances for the case of a random distribution of particles. It is shown that the nondivergent part of the atmospheric motions gives rise to a random distribution of initially regularly spaced particles. Departures from the random distribution are therefore produced by the divergent part of the atmospheric motions. In the experiment they resulted in the increase in distances from random points in space to the nearest constant-volume particle of about 12 and 4 per cent, at the levels corresponding to 800 and 300 mb, respectively. The computational region was approximately equal to the area north of 15N; a somewhat larger effect of the divergent part of the wind should be expected in the case of the global constant-volume trajectories.

1. Introduction

It is generally considered that the sparsity of upper-air observations is one of the major obstacles for the further improvement of numerical weather analysis and forecasting, if not actually the most acute one. Huge areas of the globe are totally inadequately covered by the data. Also the accuracy of the data is not satisfactory; with an increased coverage we still can not measure the divergent part of the wind in a reliable way. There is little hope that the situation can be significantly improved using present methods of upper-air observations.

One fresh possibility to overcome this data problem is given by the idea of using superpressure balloons for upper-air observations. The system, Global HOrizontal Sounding Technique (GHOST), is outlined for instance in the paper by Lally (1960), and has been much advanced since. The balloons can remain aloft for more than a month, emitting necessary information, and being tracked by satellites. They would not provide a hazard to aircraft.

In this connection a problem arises—what will be the space distribution of a large number of balloons, floating at the constant-volume surfaces? One would not like to have the divergent part of the air motions creating large holes without any balloons. At the same time the problem is academically interesting, as being complementary to the large-scale two-dimensional diffusion. Instead of investigating how a cluster of marked particles is diffusing to eventually realize a homogeneous distribution of particles in space, we focus our attention on the process of destroying an initially existing homogeneous distribution of marked particles, subject to the two-dimensional motion. While the former process depends primarily on the deformation properties of fluid motion (Djurić, 1963), the latter has to depend on the balance between the divergent part of the motion, tending to destroy the homogeneous spacing of marked particles, and the deformation part of the motion, tending to re-establish such a spacing of particles.

With the purpose of investigating this problem, a numerical experiment has been performed: a very large number of diagnostic trajectories has been computed for a 30-day time period. The method and results of the experiment are presented in this paper. Computations have been based on the National Meteorological Center numerical analysis data. The investigation has several by-products; for instance, some problems of trajectory computations are considered in more detail, and the mean 30-day meridional circulation has been computed, as being the forcing mechanism for the meridional distribution of the considered marked constant-volume particles. In connection with the statistical description of the results, contributions have been made to the theory of the distribution of distances to the nearest neighbor among a large number of particles.

To our knowledge all so far reported trajectory computations have been done using the non-divergent velocity components only, and therefore can not serve to compare the obtained results. Experiments similar to this one have, however, been simultaneously carried out by

J. K. Angell, of the U. S. Weather Bureau, and by Y. Mintz, of the University of California at Los Angeles. Angell's computations are also made with the use of the National Meteorological Center data; Mintz's computations, however, are based on his two-level global general circulation model. Meteorological convenience of the observations made with the use of quasi-horizontally floating balloons has been extensively discussed by Angell (1961).

2. Scheme of the experiment

The scheme of the computations can be described as consisting of the following steps:

a. Interpolation of the data to a chosen isopycnic surface. National Meteorological Center data (temperatures and heights of the pressure surfaces) have been available at five standard pressure levels, in grid points of its 1977-point octagonal grid. To compute the isopycnic trajectories it is desirable to have the data at a chosen isopycnic surface. To this end vertical interpolation at each grid point was performed, using the assumption

$$T=a+bz+cz^2. \tag{1}$$

Here T is the absolute temperature and z is the height. Coefficients a, b and c have been computed by fitting (1) to the values of T and z at the three nearest standard pressure surfaces. Thus the temperature was a prescribed function of height; assuming the hydrostatic relationship, pressure and density as functions of height are then determined, except for an arbitrary constant. This constant was taken to be the pressure of the nearest standard pressure surface, at its observed height.

b. Computation of the non-divergent velocity components. For the use of the data at a constant density surface, an x, y, ρ, t-system can be defined in the way analogous to the definition of the commonly used x, y, p, t-system. Making use of the hydrostatic equation, and having the subscripts indicate which variable is held constant in the process of differentiation, we obtain

$$\frac{1}{\rho}\nabla_z p=\nabla_\rho(gz+RT). \tag{2}$$

Here g is the acceleration of gravity, and R is the gas constant. Equations of motion and the balance equation in the ρ-system will therefore have the same form as those in the p-system, except for the potential

$$\xi=gz+RT$$

standing in place of the geopotential $\phi=gz$.

This being so, the following approximate form of the balance equation

$$\nabla^2\xi-\frac{1}{f}\nabla f\cdot\nabla\xi-f\nabla^2\psi=0 \tag{3}$$

has been solved, to obtain the stream function ψ. Subscripts ρ are dropped in (3) and mostly later in the text, and f is the Coriolis parameter.

Stream function values have been differentiated with the use of the second-order difference formula (Thompson, 1961) to compute the non-divergent velocity components

$$\mathbf{v}_1=\mathbf{k}\times\nabla\psi.$$

Here $\mathbf{k}$ is the vertical unit vector. To enable the application of the second order formula, stream function values have been extrapolated two rows of grid points out of the 1977-point grid boundary, by a combination of linear extrapolation and smoothing.

c. Computation of the divergent velocity components. The ω-equation (in p-system) has been solved, giving the values of the $\omega=dp/dt$ at four pressure levels, along with the values at the two boundary levels at the top and at the bottom of the atmosphere. The procedure used for solving the ω-equation is given with more detail in the following separate section. A second order polynomial

$$\omega=A+Bp+Cp^2 \tag{4}$$

was then fitted to the three nearest values of ω. Using (4) the values of

$$\mathrm{div}_p\mathbf{v}=-\frac{\partial\omega}{\partial p}$$

have been obtained at the considered constant density surfaces.

Making use of (2) we can see that the isopycnic divergence is related to the isobaric divergence by the equation

$$\mathrm{div}_\rho\mathbf{v}=\mathrm{div}_p\mathbf{v}+R\rho\nabla_\rho T\cdot\frac{\partial\mathbf{v}}{\partial p}. \tag{5}$$

At the same time the thermal wind equation can, in terms of $\nabla_\rho T$, be written in the form

$$\frac{\partial\mathbf{v}_g}{\partial p}=-\frac{g-R\gamma}{fg\rho T}\mathbf{k}\times\nabla_\rho T, \tag{6}$$

where $\gamma=-\partial T/\partial z$ is the lapse rate of temperature, and $\mathbf{v}_g$ the geostrophic wind. Hence, the second term on the right side of (5) is equal to zero when $\partial\mathbf{v}/\partial p$ is parallel to $\partial\mathbf{v}_g/\partial p$. We have, therefore, assumed the horizontal divergence in the considered isopycnic surfaces to be equal to the corresponding horizontal divergence in isobaric surfaces.

From the fields of divv the velocity potential fields have been obtained by solving the Poisson's equation

$$\nabla^2\chi=\mathrm{div}\mathbf{v}, \tag{7}$$

where χ is the velocity potential. Eq. (7) was solved with the lateral boundary condition $\chi=0$, and with the use of the nine-point difference approximation to $\nabla^2\chi$.

Velocity potential values have been differentiated using the usual centered first derivative difference formula to compute the divergent velocity components

$$\mathbf{v}_2=\nabla\chi.$$

To enable the application of the centered difference formula, velocity potential values have been linearly extrapolated one row of grid points out of the 1977-point grid boundary.

d. Trajectory computations and statistics of the results. Numerical details of the trajectory computations are given in Section 4. Also the method for the statistical description of the results and its application are presented later, in Sections 6 and 7.

3. The ω-equation

The scheme for solving the quasi-geostrophic form of the ω-equation was designed by John A. Brown, Jr., at the National Center for Atmospheric Research, for his use in diagnostic energy studies. A change was made in the computation of the lower boundary condition, so as to incorporate the effect of the flow toward the lower pressure at the ground. This change, however, did not make much difference in the results.

The equation had the form

$$\sigma\nabla^2\omega+f_0^2\frac{\partial^2}{\partial p^2}(\omega+\omega_f)=f_0\frac{\partial}{\partial p}(\mathbf{v}\cdot\nabla\eta)-\nabla^2\left(\mathbf{v}\cdot\nabla\frac{\partial\phi}{\partial p}\right), \quad (8)$$

where $\sigma=-\alpha\partial\ln\theta/\partial p$ is the static stability parameter, α being the specific volume and θ the potential temperature; f_0 is the value of the Coriolis parameter at 45N latitude, η is the absolute vorticity, and at the ground level

$$\omega_f=-\frac{g\rho}{f_0}\mathbf{k}\cdot\nabla\times(C_d|\mathbf{v}|\mathbf{v}), \quad (9)$$

C_d being the skin drag coefficients (Cressman, 1960). When solving (8) the terms on the right side have been computed using the approximate balance equation of the form analogous to (3), σ was considered to be a function of pressure only, and ω_f was considered equal to zero at all computation levels above the ground.

To compute ω_f and the lower boundary value of ω, the wind at the ground level was needed. It was obtained by first linearly extrapolating the geostrophic wind to the ground, and then computing the wind which results from the assumptions that (a) the acceleration is zero, and (b) the stress is at the ground proportional to the square of the wind speed [this is the assumption underlying (9)] and decreases linearly with decreasing pressure, so as to drop to zero after a pressure decrease of Δp. In such a case the wind at the ground level has a cross-isobar angle

$$\beta=\arccos\{2B[(1+B^2)^{\frac{1}{2}}-B]\}^{\frac{1}{2}}, \quad (10)$$

where

$$B=\frac{f\Delta p}{2C_d\rho g|\mathbf{v}_g|},$$

and the magnitude

$$|\mathbf{v}|=|\mathbf{v}_g|\cos\beta. \quad (11)$$

Δp has been set equal to 238 mb: this is the pressure difference from the ground to the nearest level of the scheme for solving (8).

Having computed the wind at the ground level the corresponding values of ω have been obtained by imagining that the atmosphere extends everywhere to 1013 mb, and that the vertical motion ω_m at that level is induced according to the flow of this ground level wind up or down the slope of the actual terrain. Hence,

$$\omega_m=\mathbf{v}\cdot\nabla p_m, \quad (12)$$

where p_m is the standard pressure at the surface of the ground. A constraint was furthermore imposed that the area average of the ω_m be equal to zero, to counteract the spurious effect of systematically obtaining the positive values of the area average of ω_m, as a result of predominantly downslope motion in the middle-latitude Ferrel cell. This constraint is, as follows from the continuity equation, equivalent to setting the total mass outflow through the lateral boundary equal to zero.

4. Some aspects of trajectory computations

With known components of the wind $\mathbf{v}(u,v)$ at a set of discrete grid points in space and time, two methods have previously been used for the air trajectory computations. In a straightforward way we can compute the trajectories by solving the system of equations

$$dx/dt=u(x,y,t), \quad dy/dt=v(x,y,t). \quad (13)$$

Another possibility is to compute the time change in individually conserved Lagrangian coordinates a and b, as discussed and applied by Djurić (1961) and Wiin-Nielsen (1959). Then we have to solve the equations

$$\partial a/\partial t=-\mathbf{v}\cdot\nabla a, \quad \partial b/\partial t=-\mathbf{v}\cdot\nabla b. \quad (14)$$

The advantage of this latter method is that the computations are done in the grid points, and so no space interpolation is needed as long as we do not want to know where some particular material points are. However, to keep the truncation errors small we have to redefine the fields of a and b at intervals of about 12 hr, and then we do have to interpolate fields of a and b if we want to keep track of the motion of a particular set of points. The price of using the partial instead of ordinary differential equations is paid by having to define the boundary conditions for the fields of a and b.

Mostly in view of the problems at the lateral boundary the former straightforward method seemed to be more convenient for the purpose of our experiment, and has therefore been used. The numerical scheme is

given in the remaining part of this section. We have here defined the trajectories to be two-dimensional; there would mostly be no essential differences in the case of three-dimensional trajectories.

Time interpolation. Since the subsequent data fields are available at time intervals of 12 hr, time interpolation of the data is desirable if we want to use time steps shorter than 12 hr for the numerical solution of (13). To interpolate a variable α it seems most suitable to assume that

$$\alpha(t)=a_0+a_1t+\cdots+a_nt^n, \tag{15}$$

and we can for each grid point compute the coefficients $a_0, a_1, \cdots, a_n$ so to fit $n+1$ known values of α at this point, $\alpha(t_0), \alpha(t_1), \cdots, \alpha(t_n)$.

In computations reported here, velocity components have been interpolated in time. This was done with the use of (15) and fitting three subsequent velocity fields—two of them preceding and one being after the interpolation time.

Space interpolation. When solving (13), velocity components at points between the points of the grid are in general needed. Having a square grid, the simplest interpolation formula should make use of the values at four surrounding grid points. The formula in common use can be written as

$$\alpha(p,q)=(1-p)(1-q)\alpha(0,0)+p(1-q)\alpha(1,0)+q(1-p)\alpha(0,1)+pq\alpha(1,1). \tag{16}$$

Here α is the interpolated variable, grid distance is the unit of length, and coordinate system p,q is put with the origin in one of the four surrounding grid points and axes parallel to the grid lines. Eq. (16) was used for the space interpolation of velocity components in our experiment.

Finite difference scheme. Many finite difference schemes can successfully be used for the solution of (13); they will only require different computation time to achieve the same average accuracy. Two schemes have been tested, requiring very nearly the same computation time per time step.

Let us have superscripts denote the number of time steps Δt elapsed, and, for brevity, introduce the symbol

$$x_n=x^k+n\Delta tu[x^k,y^k,(k+\tfrac{1}{2})\Delta t],$$

with the analogous meaning for y_n. Being so, we define "scheme A" by

$$x^{k+1}=x^k+\Delta tu[x_{\frac{1}{2}}, y_{\frac{1}{2}}, (k+\tfrac{1}{2})\Delta t], \tag{17}$$

and "scheme B" by

$$x^{k+1}=x^k+(\Delta t/2)\{u[x_0, y_0, (k+\tfrac{1}{2})\Delta t]+u[x_1, y_1, (k+\tfrac{1}{2})\Delta t]\} \tag{18}$$

with again the analogous formulae for y^{k+1}. Using the same 0.908 kg m^{-3} velocity fields, 49 three-day trajectories have been computed with the use of different time steps and both of the two schemes. Trajectories computed with 2-minute time steps were defined as "exact," and so the root-mean-square error of the longer time step trajectories obtained. The results are shown in Fig. 1. Scheme B, although demanding slightly more of the actual computing work, involved larger truncation errors. Scheme A was therefore used for the further computations.

Generations of new marked points. Several computations have been made, starting with a different number of points inside the boundary of the grid. In all computations it was assumed that outside of the boundary a constant concentration of marked points existed, equal to the average initial concentration of points inside of the boundary. This assumption was realized by keeping track of the area entering through each of the segments connecting two adjacent boundary grid points, and having the marked points generated on those segments at proper moments. When having a point generated it was placed on the boundary segment at random, taking care, however, not to place it on the outflow part of the segment, should such a part exist.

5. Description of the results

Trajectories have been computed for the period 00 GMT 5 December 1962 to 00 GMT 4 January 1963. One computation was done for the 0.908 kg m^{-3} level, which is the density corresponding to the pressure of 700 mb in the U. S. Standard Atmosphere. In that computation, trajectories have been originated in the 1977 grid points, and computed with the use of the nondivergent velocity components only. Computations using the total velocity components have been performed

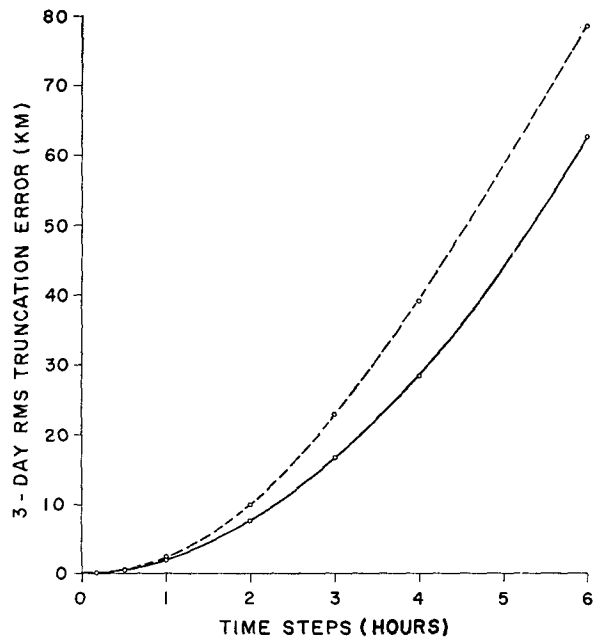

FIG. 1. Root-mean-square truncation error of 49 three-day trajectories, computed with the use of "scheme A" (full line) and "scheme B" (dashed line).

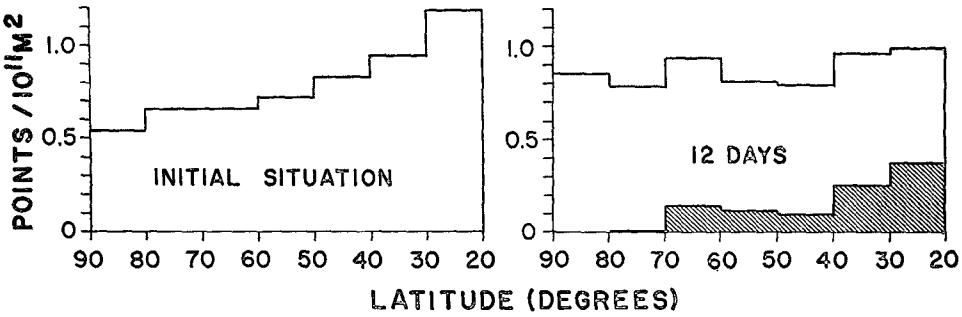

FIG. 2. Histograms of the concentration of marked points initially and after 12 days, for the 0.908 kg m^{-3} computation. The shaded area represents the contribution of the points which entered the computation area through its lateral boundary.

for the 0.458 and 1.012 kg m^{-3} levels, corresponding to the Standard Atmosphere pressures of 300 and 800 mb, respectively. These computations have been done starting with both 1908 and 954 points, put at random inside the boundary of the 1977-point grid. The number 1908 makes the initial concentration of points equal to the average concentration of the grid points in the 1977-point grid. Time steps in the trajectory computations have been chosen as to have 4, 5 and 7 time steps per 6 hr at the 1.012, 0.908 and 0.458 kg m^{-3} levels, respectively.

The computation made with the use of the non-divergent velocity fields is of interest as an illustration of the large-scale meridional mixing only, with no interference of the mean meridional circulation which is found in the divergent velocity fields. Initially the concentration of marked material points increased with decreasing latitude, being about twice as great near the boundary as in the vicinity of the pole. Consequently, an eddy poleward transport of points existed, producing a fairly constant concentration of points in about two weeks. Histograms of the concentration of points initially and after 12 days are shown in Fig. 2. Approximately the same time was needed for the first of the points entering through the lateral boundary to come in the vicinity of the pole.

Results of the computations made using the total velocity fields are given in Fig. 3. It shows the positions of the trajectory points at the two levels and at various time intervals. No contours of the continents are given, since the grid with the contours has been often reproduced previously, originally in the paper by Cressman (1959). The area within the boundary of the grid is approximately equal to the global area north of the 13.5N latitude. Maps of the positions of points are computer-produced, and therefore the points in Fig. 3 have a tendency to organize into parallel lines. In the mapping program 15 printing places have been available per each grid point, i.e., about 30 places per each trajectory point. In the few cases in which more than one point still fell into the same printing place, the extra points have been shifted to their nearest empty place.

Examination of the trajectory outprints in Fig. 3 shows that the process of clustering and dispersion of the marked particles was more effective at the lower level. Not many pronounced clusters formed; when they did form it was possible to follow their motion for some time—usually several days. In the extreme case (cluster in the left half of the 10-day, 1.012 kg m^{-3} outprint) a cluster was distinguishable for approximately ten days. It dispersed after first being stretched into a zonally oriented band. Relatively large holes with no marked particles were developing in the lower level subtropical divergence region. An enormous number of trajectory points, or a different computation method, would, however, be necessary for reliable identification of the centers having a minimum concentration of points.

The different intensity of the clustering process at the two levels does not seem to have been a result of the difference in the corresponding divergence fields. The area and time averages of the absolute values of divv have been computed for the two levels; they have been very nearly the same, 2.32 10^{-6} sec^{-1} at the 0.458 kg m^{-3} level and 2.39 10^{-6} sec^{-1} at the 1.012 kg m^{-3} level. Instead, difference in the intensity of the clustering process must have been mostly produced by the different intensity of the non-divergent motions, which tend to destroy spatial differences in concentration of marked particles. Large-scale dispersive properties of the atmosphere are mostly due to its deformation field, which is likely to intensify with height as the average wind speed increases.

Besides taking part in the formation of transient clusters and holes, the marked constant-volume particles underwent a longer time-scale meridional rearrangement, so as to conform to the prevailing meridional velocity profile. This is illustrated in Fig. 4, where the meridional profiles of divv and of the average concentration of particles in 10-degree latitude belts are shown. Histograms of the concentration represent the average values computed from the 15, 20, 25 and 30-day distributions. Given a quasi-steady meridional velocity profile, and a prescribed concentration of marked particles outside of the boundary, particles will approach some quasi-steady meridional distribution in which the convective transport of particles by the mean

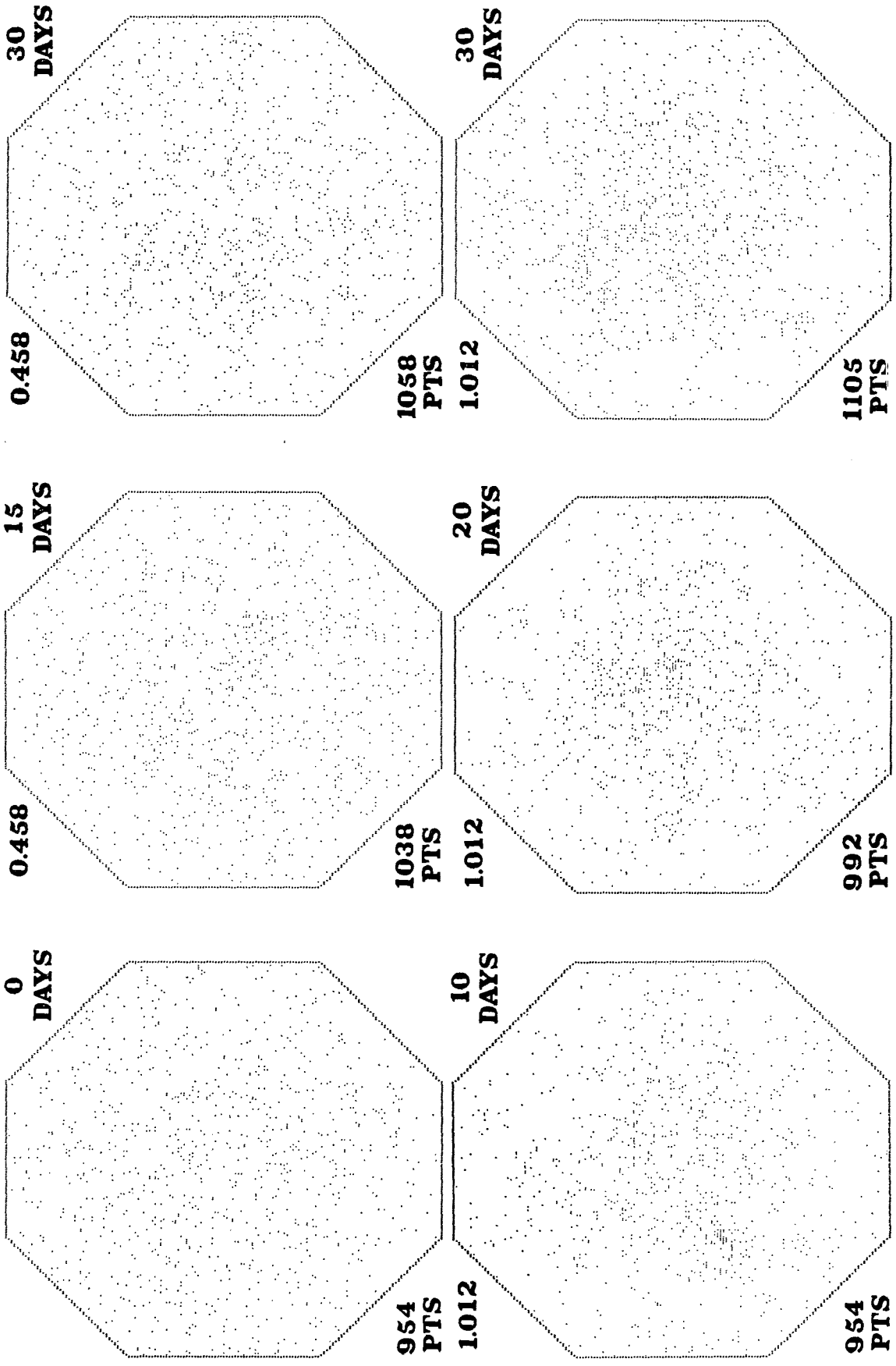

FIG. 3. Positions of the marked constant-volume points for the 0.458 kg m^{-3} (top row) and 1.012 kg m^{-3} (bottom row) 954-point computations. Both computations have been started with the same set of points, put at random inside the boundary of the grid. Points having a constant concentration on the spherical earth will on the stereographic plane have at the pole a concentration about twice as great as near the boundary of the grid. This is approximately the case for the initial spacing of points.

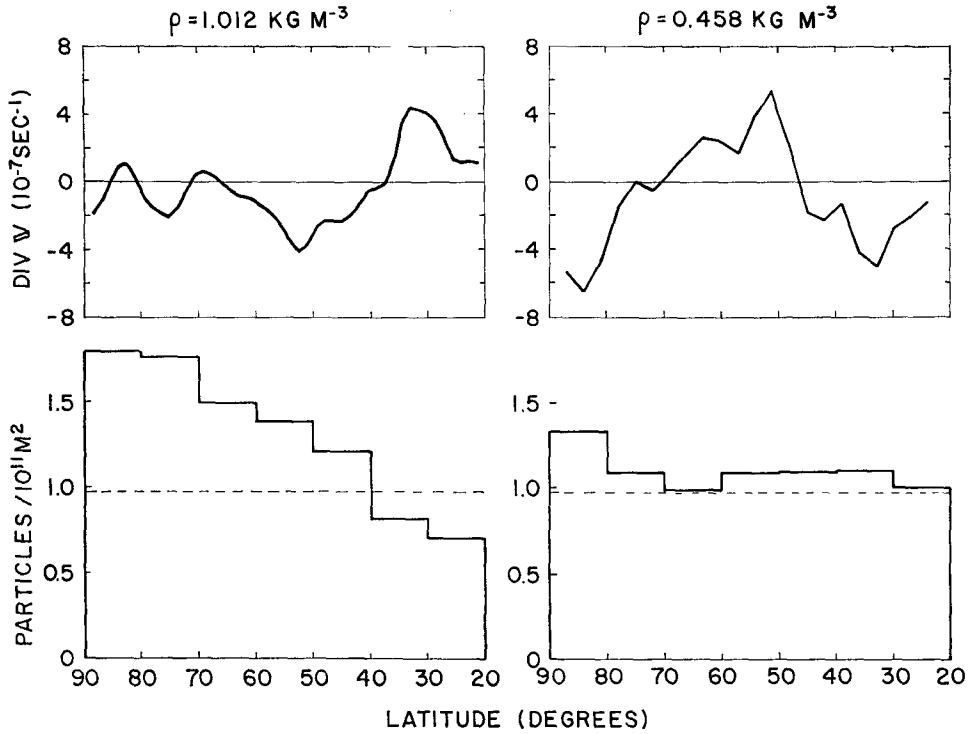

FIG. 4. 30-day average profiles of divv and average histograms of constant-volume particles. Histograms are computed from the results of the 1908-point computations. Dashed line represents the initial concentration of 0.975 particle per 10^{11} m^2, assumed to exist outside of the boundary during the trajectory computations.

meridional motion is counteracted by the equal and opposite eddy transport of particles. Such a quasi-steady meridional distribution has been reached at 0.458 kg m^{-3} level after about 15 days; at the 1.012 kg m^{-3} level, however, the quasi-steady distribution has still not been reached even after the 30 days, although it has already been approached fairly closely.

Converting values of ω into vertical velocities through the assumption $\omega = -g\rho w$ the average meridional velocity profile has been obtained, as shown in Fig. 5. The familiar three-cell pattern can be seen, with well-organized middle-latitude Ferrel cell and low-latitude Hadley cell, and less well organized polar Hadley cell. The polar cell was also not well organized in the recent study by Miyakoda (1963). The three-cell circulation did not exist regularly in instantaneous data sets processed for our experiment; for instance, in 13 out of 61 of them at the lateral boundary outflow was obtained

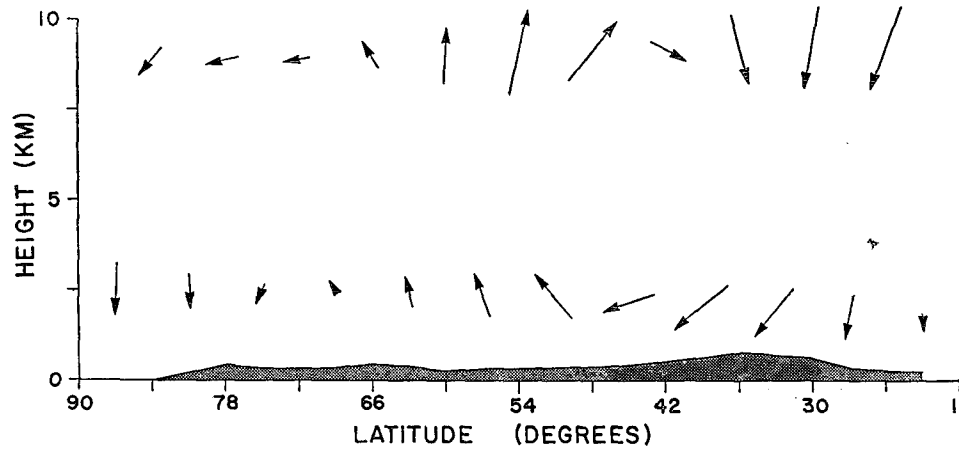

FIG. 5. 30-day mean meridional circulation (approximately for December 1962). Arrows represent the displacements in 10^6 sec (about 11.6 days), computed using the velocity components in average at their mid-points.

at the upper level and inflow at the lower level, compared to 33 cases where the opposite was true.

6. Theory of the distances to the nearest neighbor

There are several possibilities of giving a statistical description of the spacing of the considered material points. One has already been used when the concentration of points as a function of latitude was discussed. This, however, gives almost no information on the process of clustering of points. Considering the practical interest in this process, we are probably primarily interested in knowing how it will affect the distances from the points of some numerical analysis grid to our trajectory points. Having the trajectory points simulate the constant-volume sounding balloons, we would not like them to be far from the grid points. Some useful conclusions about such distances can be reached by a theoretical approach alone.

Let us first consider an infinite number of marked points distributed at random on a plane. Suppose we have a set of some other independently chosen points; to each of those there corresponds a distance at which the marked point nearest to it is found. We concentrate on the frequency function of those distances. We may also consider the distances from the marked points to the nearest neighboring marked point; since the number of marked points is infinite and they are distributed at random, the two types of distances will have the same frequency function. Expression for such a frequency function has been derived by Hertz (1909) for the general case of points in an n-dimensional space. Different derivations for the points on a plane can be found in a book by Parzen (1962) and in a previous note by the author (Mesinger, 1962). It is seen that the frequency function of the distances to the nearest marked point has the form

$$f(r)=2\pi r\chi e^{-\pi r^2\chi}, \tag{19}$$

where r stands for the distances from our reference points, and χ is the mean rate at which the marked points are distributed per unit area.

The mean value of those distances

$$\bar{d}=\int_0^\infty rf(r)dr$$

is after (19) equal to

$$\bar{d}=0.5\chi^{-\frac{1}{2}}. \tag{20}$$

It is suitable to choose the unit of length so as to make $\chi=1$; in that case we have

$$\bar{d}=0.5. \tag{21}$$

When having a finite number of marked points distributed at random on a sphere the frequency function and the mean distance will depend on the actual number of marked points. We then also have to make the difference whether we choose as reference points the marked points themselves, or some other independent set of points. Namely, denoting the number of sets of points involved by subscripts and the radius of the sphere by a, the two types of mean distances

$$\bar{d}_1=\int_0^{a\pi} rf_1(r)dr$$

and

$$\bar{d}_2=\int_0^{a\pi} rf_2(r)dr$$

will not be the same for a particular number of marked points N. Instead, we will have

$$\bar{d}_1(N+1)=\bar{d}_2(N).$$

The analysis analogous to the one for the plane case (Mesinger, 1962) shows that on a sphere

$$f_2(r)=\frac{N}{2^N a}\sin\frac{r}{a}\left(1+\cos\frac{r}{a}\right)^{N-1}. \tag{22}$$

When substituted into the preceding expression for $\bar{d}_2$ this gives

$$\bar{d}_2=a\pi\frac{1\cdot3\cdot5\cdots(2N-1)}{2^N N!}. \tag{23}$$

If we again choose the unit of length so as to have $\chi=N/4a^2\pi=1$ we obtain

$$\bar{d}_2=(N\pi)^{\frac{1}{2}}\frac{1\cdot3\cdot5\cdots(2N-1)}{2^{N+1}N!}. \tag{24}$$

From (24) it is easily seen that for all N we have $\bar{d}_2(N+1)/\bar{d}_2(N)>1$; $\bar{d}_2(N)$ is so a monotonic increasing sequence. With the aid of the Wallis product formula we, moreover, see that

$$\lim_{N\to\infty}\bar{d}_2(N)=0.5,$$

as can be expected.

Compared to the plane case we here have two opposite effects: first, points have only a limited area available, which makes the large distances less probable and distances larger than $a\pi$ impossible, and, second, a smaller area is found within the same distance from a reference point. The first effect is seen to be of more importance for all the values of N, since the values of $\bar{d}_2(N)$ are always less than 0.5. They, however, approach 0.5 rather fast with increasing N, as shown by the following values, computed after (24):

$N=$	1	10	100	1000
$\bar{d}_2=$	0.44311	0.49379	0.49938	0.49994.

The values of $\bar{d}_2$ would differ from 0.5 somewhat more when having the points on a part of a sphere only, but the difference would still be extremely small when the

number of points is of the order of the number of trajectory points in our experiment.

The spacing of our trajectory points is likely to be different from the one described by (19) more due to fact that the distribution of points will not be a random one. Marked points floating with the divergent wind will rather form a distribution where the concentration of points is a function of space coordinates, say $\chi=\chi(x,y)$. Otherwise, however, we may expect the points to be organized at random relative to each other, at least after some time if they initially were not. We shall therefore consider the frequency functions of the two types of distances for such a case. When having an independent set of reference points we now define these points to be homogeneously distributed with an infinite concentration. Actually only the distances from such independently chosen reference points seem to be of interest for the balloon-clustering problem; there are, however, some other applications (Parzen, 1962) where the distances between the marked points themselves are considered. It may so be useful to discuss both kinds of distances. We shall restrict ourselves to the frequency functions representative for a limited area A, in which a very large number of marked points is found.

To write the expressions describing the dependence of these frequency functions on $\chi=\chi(x,y)$, let us observe that in the definition of the concentration

$$\chi=\delta n/\delta A, \tag{25}$$

δA has to be a "small" area, but still large enough to contain many marked points δn, in order to make χ a smooth function of space. So the scale of space changes in χ is necessarily greater than $\delta A^{\frac{1}{2}}$. At the same time the scale of distances to the nearest marked point is less than $\delta A^{\frac{1}{2}}$. Thus, concentration can be considered constant on the scale of those distances, and relation (19) describes the probabilities of finding different nearest-point distances as a function of $\chi(x,y)$. If desired we may think of x and y as being the spherical coordinates of the earth; since a very large number of marked points is assumed, relation (19) will still hold.

So, when we consider the area

$$A=\int_A dA,$$

the frequency function of the distances from every marked point to its nearest neighbor will be equal to

$$f_1(r)=\frac{1}{N}\int_A 2\pi r\chi^2(x,y)e^{-\pi r^2\chi(x,y)}dA, \tag{26}$$

where

$$N=\int_A \chi(x,y)dA$$

is the total number of marked points found in the area A.

On the other hand,

$$f_2(r)=\frac{1}{A}\int_A 2\pi r\chi(x,y)e^{-\pi r^2\chi(x,y)}dA \tag{27}$$

will be the frequency function of the distances from the homogeneous reference points to the nearest marked point. Both of the frequency functions, $f_1(r)$ and $f_2(r)$, reduce of course to $f(r)$ when $\chi=$ const.

The mean value of the distances from every marked point to its nearest neighbor

$$\bar{d}_1=\int_0^\infty rf_1(r)dr,$$

and the mean value of the distances from the homogeneous reference points to the nearest marked point

$$\bar{d}_2=\int_0^\infty rf_2(r)dr$$

after (26) and (27) are equal to

$$\bar{d}_1=\frac{1}{2N}\int_A \chi^{\frac{1}{2}}(x,y)dA \tag{28}$$

and

$$\bar{d}_2=\frac{1}{2A}\int_A \chi^{-\frac{1}{2}}(x,y)dA. \tag{29}$$

Both of the mean distances, $\bar{d}_1$ and $\bar{d}_2$, reduce again to $\bar{d}$ when $\chi=$ const.

It is of interest to look for the extreme values of the distances $\bar{d}_1$ and $\bar{d}_2$ under the constraint that the average concentration

$$\bar{\chi}=\frac{1}{A}\int_A \chi(x,y)dA$$

remains constant. Using the technique of the calculus of variations, it can be shown that the distances $\bar{d}_1$ and $\bar{d}_2$ have then the stationary values only when the concentration is spatially constant, i.e., everywhere equal to N/A. It is further seen that at such constant concentration $\bar{d}_1$ has its maximum value, and $\bar{d}_2$ its minimum value. So, choosing the unit of length so as to make the average concentration equal to 1, 0.5 will be the maximum value of the mean nearest neighbor distance $\bar{d}_1$, and at the same time the minimum value of the mean nearest marked point distance $\bar{d}_2$.

The mean distances $\bar{d}_1$ and $\bar{d}_2$ may also have non-stationary extreme values. The mean distance $\bar{d}_1$ will obviously have its minimum value, equal to 0, when all the marked points are in the same arbitrarily placed point. The mean distance $\bar{d}_2$ will have its maximum value again when all the marked points are in the same point, but this time it has to be suitably placed, its position depending on the particular form of the area A.

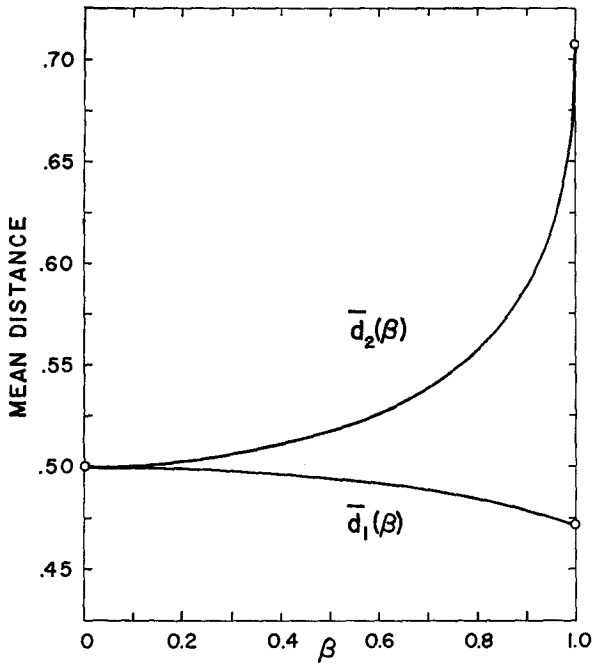

FIG. 6. The mean distances $\bar{d}_1$ and $\bar{d}_2$ when the area A is defined by $-a \leqq x \leqq a$, $-b \leqq y \leqq b$, and the concentration equal to $1+\beta x/a$.

These extreme values occur for non-continuous functions $\chi(x,y)$, when Eqs. (26) and (27) are no longer valid.

As an example of the possible changes in $\bar{d}_1$ and $\bar{d}_2$ they have been computed for the case when inside a square region $-a \leqq x \leqq a$, $-b \leqq y \leqq b$, concentration is a linear function of x, given by $\chi = 1+\beta x/a$. The results, shown in Fig. 6, indicate that both mean distances are rather conservative, especially the mean nearest-neighbor distance $\bar{d}_1$. The mean nearest-point distance $\bar{d}_2$ is rising sharply in the vicinity of $\beta = 1$, since then the concentration becomes zero for $x = -a$, producing after (29) infinite values of d_2.

We can also obtain expressions for the n-th moment of the distribution of d_1

$$\mu_1^{(n)} = \int_0^\infty r^n f_1(r)dr$$

and d_2

$$\mu_2^{(n)} = \int_0^\infty r^n f_2(r)dr.$$

Substituting (26) and (27) into these definitions we find

$$\mu_1^{(n)} = \frac{n\Gamma\left(\frac{n}{2}\right)}{2N\pi^{n/2}} \int_A \chi^{1-(n/2)}(x,y)dA \tag{30}$$

and

$$\mu_2^{(n)} = \frac{n\Gamma\left(\frac{n}{2}\right)}{2A\pi^{n/2}} \int_A \chi^{-(n/2)}(x,y)dA. \tag{31}$$

From (30) we see that the second moment of the distribution of d_1 is equal to

$$\mu_1^{(2)} = 1/\pi\bar{\chi}, \tag{32}$$

and is therefore independent of the form of $\chi(x,y)$. It follows from (32) and from the definition of a frequency function that two different functions $f_1(r)$ have to intersect each other at least twice. Furthermore, substituting $n+2$ instead of n into (30) we obtain

$$\mu_2^{(n)} = \frac{2\pi\bar{\chi}}{n+2}\mu_1^{(n+2)}, \tag{33}$$

or, specially for $n = 1$,

$$\bar{d}_2 = \tfrac{2}{3}\pi\bar{\chi}\mu_1^{(3)}. \tag{34}$$

7. Application to the spacing of computed trajectories

It seems reasonable to expect the non-divergent part of the wind to bring forth and maintain a random distribution of initially organized and floating particles. The time-scale of this process of destroying an organized spacing of a set of particles may be regarded as an indicator of the intensity of the turbulence in the wind field; namely it is the turbulent character of the motion which gives rise to the change in the position of floating particles relative to each other. Richardson (1926) described how such a process would be illustrated in his distance-neighbor graph. In the cited note of the author (Mesinger, 1962) the mean values and the frequency functions of the nearest-neighbor distances have been used to illustrate it for 500 mb, 8-day barotropically forecasted trajectories. Here we shall do it with more rigor for the 0.908 kg m^{-3} non-divergent computation.

The initial concentration of marked particles was at the 0.908 kg m^{-3} level proportional to the square of the map factor of the stereographic projection, increasing therefore from the center toward the boundary of the

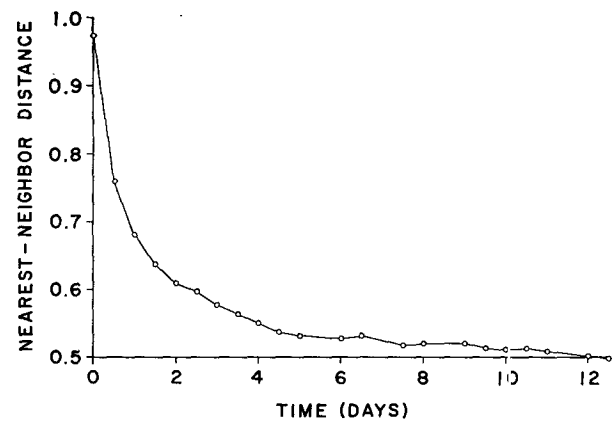

FIG. 7. The mean values of the distances to the nearest neighbor, for the non-divergent, 0.908 kg m^{-3} trajectories. Trajectories have been originated in the points of the National Meteorological Center 1977-point grid.

region. In addition, particles were spatially organized relative to one another, since they made a square grid in the image surface of the projection. To produce a random distribution, non-divergent air motions had to (a) accomplish spatially constant concentration through the poleward eddy transport of marked particles, and (b) completely destroy their organized spacing relative to one another. The two processes obviously need not have the same time rate, the process (a) depending on the meridional gradients of the concentration, and (b) depending on the concentration itself. If and when both of these processes are completed, distribution of marked particles will be random, and the frequency function of distances to the nearest of them has to conform with (19).

To gain more insight into this question, the mean values and the frequency functions of nearest neighbor distances have been computed at various time intervals. Distances have been computed only for particles which happened to be inside an inner boundary, put two rows of grid points inside the 1977-point grid boundary. This practically excludes the influence of the fact that there have been no points outside of the 1977-point boundary. Unit of length was always chosen so as to make the average concentration of marked particles inside the inner boundary equal to 1.

The obtained mean values of the nearest neighbor distances, as a function of time, are partly shown in Fig. 7, which illustrates the time rate of the process of destroying the initially organized relative spacing of particles. The period shown in Fig. 7 approximately corresponds to the one they needed to complete the other process of realizing a latitude-independent concentration; we see that their random relative spacing was not accomplished before that, since it is only the organized relative spacing of particles that can make the mean nearest neighbor distances be systematically greater than 0.5. After this 12.5-day period the mean distances oscillated about the random distribution value of 0.5. Histograms of the nearest neighbor distances approached the random distribution shape (19) in much the same way, deviating from it only in a randomly looking fashion after the period represented in Fig. 7. It so appears that the random spacing of particles relative to each other happened to be reached also in the period of about 12 days. The average histogram of the nearest neighbor distances, computed by averaging the 15, 20, 25 and 30-day histograms, is shown in Fig. 8. The difference between the shape of the histogram and that of the frequency function (19) appears to be slight and not a systematic one. It seems so fairly safe to conclude that the non-divergent component of the air motions does have the property of producing as well as maintaining the random distribution of floating particles.

This being so, we may describe the effect of divergence in the wind field on the spacing of trajectories by looking at the differences between the actual distribution of the

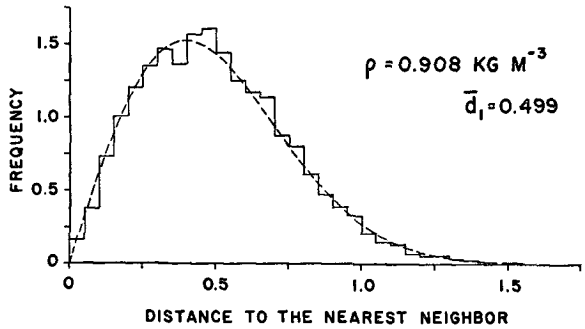

FIG. 8. Average histogram of the distances to the nearest neighbor, for the non-divergent, 0.908 kg m^{-3} trajectories. Histogram is the average of the 15, 20, 25 and 30-day histograms. The dashed curve represents the random distribution frequency function (19).

particles and the random one. When the quasi-steady meridional distribution of marked particles is realized, the histograms of the nearest-particle distances should also reach some quasi-steady shape, characteristic of the particular level and season considered. We have seen that such a quasi-steady meridional distribution has been reached at the 0.458 kg m^{-3} level after about 15 days; at the 1.012 kg m^{-3} level it has still not been reached at that time, however the histograms are not likely to have much systematic change any more. The formation of a definite meridional profile of the concentration of particles is only one of the two processes influencing the departure of the histogram shapes from the shape of the random distribution frequency function (19), the other being the formation of transient clusters and holes in the concentration fields, and having a time-scale equal to that of synoptic disturbances. The average histograms shown in Fig. 9, and computed again by averaging the 15, 20, 25 and 30-day histograms, should thus give a good representation of the final effects of divergence fields at the two levels. Histograms of the "nearest neighbor" distances are computed in the same way as the one shown in Fig. 8; the histograms of "nearest particle" distances are obtained by taking 1750 points, put at random inside the same inner boundary, to be the reference points from which the distances to the nearest marked particle are measured. Histograms are based on the 1908-point computations.

We see that, in agreement with the results of the previous section, effect of divergence fields was to give rise to a decrease in the mean distances $\bar{d}_1$ and to an increase in the mean distances $\bar{d}_2$, relative to the random distribution value of 0.5. The changes have been rather small, however, as they have also been in the example illustrated in Fig. 6. The mean distance $\bar{d}_1$, decreased 2.6 and 5.3 per cent, and the mean distance $\bar{d}_2$ increased 4.2 and 12.2 per cent, at the upper and lower levels, respectively. In both histograms of d_1 a deficiency in medium and a corresponding surplus in small as well as in large distances, relative to the random distribution curve, is observed. The shape of the histograms is so

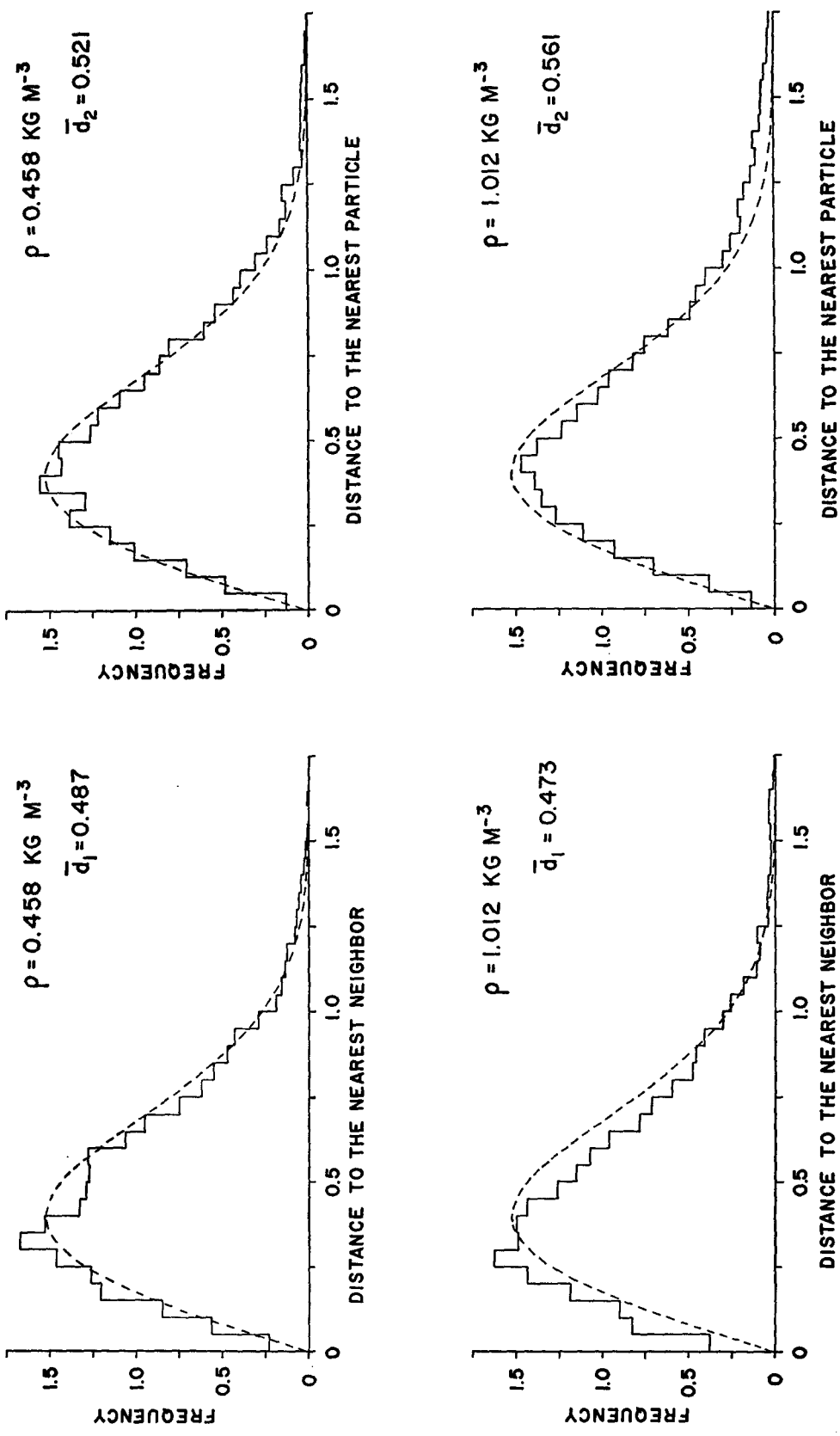

FIG. 9. Average histograms of the distances to the "nearest neighbor" and the "nearest particle" for the two divergent computations. "Nearest neighbor" distances are measured from the marked constant-volume particles themselves, and "nearest particle" distances from randomly spaced points, to the nearest marked particle. The dashed curves represent the random distribution frequency function (19).

changed more than indicated by the small change in the mean distances. Histogram shapes intersect the random distribution curve twice, and are therefore not in disagreement with (32). In the histograms of d_2 a decrease in medium and also in small distances is seen, with a pronounced relative increase in the frequency of large distances.

With the balloon-clustering problem in mind, it seems interesting to know the maximum values of the distances d_2. In the histograms which were averaged to compute the ones shown in Fig. 9, they ranged from 1.575 to 1.975 at the upper level, and from 1.975 to 2.675 at the lower level, taking mid-points of the class intervals as representative. Maximum values of the distances d_1 have been generally smaller. One should, however, expect somewhat larger maximum distances in the case of global trajectories, with no lateral boundaries, and all of the equatorial Hadley circulation included.

Available histograms offered the opportunity to check the agreement of histogram shapes with Eqs. (32) to (34) of the previous section. From the histograms at both levels and at intervals of 5 days, second moments of the distribution of d_1 have been computed. The results are given in Table 1. After (32), they should all have been equal to 0.318.

With the use of the same histograms the third moments of the distribution of d_1 have also been computed. They are plotted in Fig. 10 against the corresponding values of $\bar{d}_2$. Only a modest agreement with the line representing Eq. (34) is seen, with points showing a preference to fall on the left side of that line. At least in part this seems to be due to the fact that only a limited number of marked particles is considered, therefore no distance is larger than a particular maximum one. This has a tendency to make especially the higher moments less than they otherwise would be. The higher the moments the more they are dependent on the small number of largest distances, and, given the number of marked particles, the agreement with (33) should be expected to deteriorate with increasing n.

8. Conclusions

Computation of a very large number of non-divergent constant-volume trajectories strongly supports the expectation that the non-divergent atmospheric motions should produce and maintain a random distribution of floating and initially organized particles. It is seen that a departure from such a random distribution has to result in a decrease in the mean distances from floating particles to the nearest neighboring floating particle, and in an increase in the mean distances from some independent homogeneously spaced points to the nearest floating particle. This has been confirmed by the computed divergent trajectories. It does not, however, appear that the rather small increase in the latter type of distances could represent a serious deficiency of a constant-volume balloon observation system.

TABLE 1. Second moments of the distribution of d_1.

Days:	0	5	10	15	20	25	30	Average
0.458 kg m^{-3}	0.293	0.321	0.320	0.310	0.323	0.323	0.296	0.312
1.012 kg m^{-3}	0.293	0.302	0.307	0.300	0.305	0.312	0.321	0.306

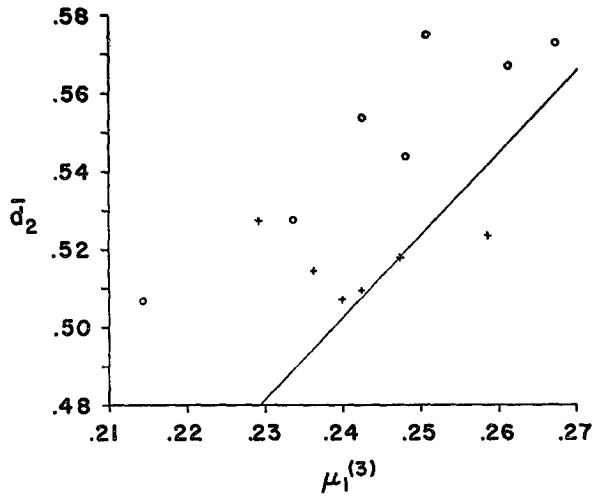

FIG. 10. Mean nearest particle distances as a function of the third moments of the distribution of nearest neighbor distances. The crosses represent the 0.458 kg m^{-3} values, and the circles the 1.012 kg m^{-3} ones. The straight line shows the theoretical dependence after (34).

The experiment performed here can also be done in an alternative way. Differentiating (25), and assuming Fickian diffusion of marked particles, we obtain

$$\partial\chi/\partial t = -\mathbf{v}\cdot\nabla\chi - \chi\,\mathrm{div}\mathbf{v} + K\nabla^2\chi, \qquad (35)$$

an equation in form analogous to the simplified vorticity equation. Here the diffusion coefficient K accounts for the diffusion on the scale smaller than $\delta A^{\frac{1}{2}}$. The Eq. (35) can now be integrated using the Eulerian or a quasi-Lagrangian technique, and then the frequency functions $f_1(r)$ and $f_2(r)$ obtained through Eqs. (26) and (27), instead by computing trajectories and distances to the actual marked particles.

Acknowledgments. This investigation has been done while the author enjoyed the hospitality extended to him at the National Center for Atmospheric Research. Its initiation has been stimulated by a discussion and encouragement from Dr. Jule G. Charney. Programs for solving the balance and the omega equation have been designed and made available to the author by Mr. John A. Brown, Jr. He also took part in many useful discussions concerning Section 3 of this paper, contributing to the material it contains. Dr. Akira Kasahara and Dr. Warren Washington kindly read the manuscript and made helpful comments and suggestions. The writer has also benefited from several comments

by Dr. George W. Platzman and from a suggestion by Dr. Irving Weiss. Miss Margaret Drake efficiently helped with many programming and computational difficulties, and Mr. Placido Jordan kindly did some of the computational work.

REFERENCES

Angell, J. K., 1961: Use of constant level balloons in meteorology. *Advances in Geophysics*, **8**, New York, Academic Press, 137–219.

Cressman, G. P., 1959: An operational objective analysis system. *Mon. Wea. Rev.*, **87**, 367–374.

——, 1960: Improved terrain effects in barotropic forecasts. *Mon. Wea. Rev.*, **88**, 327–342.

Djurić, D., 1961: On the accuracy of air trajectory computations. *J. Meteor.*, **18**, 597–605.

——, 1963: The effect of deformation in the wind field on the large-scale horizontal dispersion of clusters in the atmosphere. Darmstadt, Inst. für Meteor.—Tech. Hochsch., Contract AF 61 (052)-366, 49 pp. (Available from Defense Documentation Center, Alexandria, Va. Order No. AD 411501.)

Hertz, P., 1909: Über den gegenseitigen durchschnittlichen Abstand von Punkten, die mit bekannter mittlerer Dichte im Raume angeordnet sind. *Math. Ann.*, **67**, 387–398.

Lally, V. E., 1960: Satellite satellites—a conjecture on future atmospheric-sounding systems. *Bull. Amer. Meteor. Soc.*, **41**, 429–432.

Mesinger, F., 1962: Some problems of atmospheric diffusion on very large scale. Darmstadt, Inst. für Meteor.—Tech. Hochsch., Contract AF 61 (052)-366, 22 pp. (Available from Defense Documentation Center, Alexandria Va. Order No. AD 402328.)

Miyakoda, K., 1963: Some characteristic features of winter circulation in the troposphere and lower stratosphere. Chicago, Univ. of Chicago, Dept. of the Geophys. Sci., Tech. Rep. and Publ. of the Dyn. Pred. Group, No. 43, 160 pp.

Parzen, E., 1962: *Stochastic Processes*. San Francisco, Holden-Day, 324 pp.

Richardson, L. F., 1926: Atmospheric diffusion shown on a distance-neighbour graph. *Proc. Royal Soc.*, **A110**, 709–737.

Thompson, P. D., 1961: *Numerical Weather Analysis and Prediction*. New York, Macmillan, 170 pp.

Wiin-Nielsen, A., 1959: On the application of trajectory methods in numerical forecasting. *Tellus*, **11**, 180–196.